

Article

Metal-Organic Framework Fabricated V₂O₅ Cathode Material for High-Performance Lithium-Ion Batteries

 Jay Singh ^{1,†}, Kichang Hong ^{2,†}, Younggwon Cho ^{2,†}, M. Shaheer Akhtar ³ , Jungwon Kang ^{2,*} and Alok Kumar Rai ^{1,*} 
¹ Department of Chemistry, University of Delhi, Delhi 110007, India; jay.duchemistry@gmail.com

² Department of Advanced Materials Science and Engineering, Mokpo National University, 61 Dorim-ri, 1666 Yeongsan-ro, Cheonggye-myeon, Muan-gun 58554, Jeonnam, Korea; hkc8249@mnu.ac.kr (K.H.); cho4308@mnu.ac.kr (Y.C.)

³ New & Renewable Energy Materials Development Center (NewREC), School of Chemical Engineering, Jeonbuk National University, Jeonju 54896, Jeonbuk, Korea; shaheerakhtar@jbnu.ac.kr

* Correspondence: jwkang17@mokpo.ac.kr (J.K.); akrai@chemistry.du.ac.in (A.K.R.)

† These authors contributed equally to this work.

Abstract: In this article, oval-shaped V₂O₅ nanoparticles were hydrothermally synthesized using a metal-organic framework (MOF), which was then followed by calcination under an air atmosphere. The obtained sample was characterized through various characterization techniques to determine the sample purity and the structural and morphological details. Since V₂O₅ possesses a layered crystal structure, it exhibits promising electrochemical performances as a cathode material for lithium-ion battery applications. However, poor cycling and inferior rate capabilities are the major issues that limit its application. Thus, a strategy to fabricate unique oval-shaped V₂O₅ nanoparticles was employed here to improve electrochemical performances using an MOF, which acts as a template and provides a skeleton for the growth of a novel nanostructure. It is believed that the oval-shaped morphology is beneficial to achieving better electrochemical results due to the large surface area and the existence of numerous channels for lithiation and de-lithiation. The obtained electrochemical result reveals that the V₂O₅ electrode can be considered a prominent cathode material for next-generation lithium-ion battery applications.

Keywords: cathode; oval-shaped; metal-organic frameworks; Li-ion battery



Citation: Singh, J.; Hong, K.; Cho, Y.; Akhtar, M.S.; Kang, J.; Rai, A.K. Metal-Organic Framework Fabricated V₂O₅ Cathode Material for High-Performance Lithium-Ion Batteries. *Coatings* **2022**, *12*, 844. <https://doi.org/10.3390/coatings12060844>

Academic Editor: Emerson Coy

Received: 13 May 2022

Accepted: 6 June 2022

Published: 16 June 2022

Publisher's Note: MDPI stays neutral with regard to jurisdictional claims in published maps and institutional affiliations.



Copyright: © 2022 by the authors. Licensee MDPI, Basel, Switzerland. This article is an open access article distributed under the terms and conditions of the Creative Commons Attribution (CC BY) license (<https://creativecommons.org/licenses/by/4.0/>).

1. Introduction

As the modern development of society expanded, the demand for energy storage devices significantly increased. Currently, lithium-ion batteries (LIBs) are the most suitable energy storage devices, especially for portable electronics and electric vehicles [1–5]. Rechargeable LIBs are now globally used due to their environmentally friendly features, lightweight design, flexibility and high energy density. It is well-known that cathode materials largely affect not only the electrochemical performance but also the cost of LIBs. There are numerous commercially available cathode materials such as LiCoO₂ (140 mAh g^{−1}), LiMn₂O₄ (148 mAh g^{−1}) and LiFePO₄ (~170 mAh g^{−1}), which have the advantages of a high working voltage and an excellent cycling performance. However, their low theoretical capacities, as well as the high cost of materials, limit their practical applications [6–12]. Therefore, the development of a new class of cathode materials which exhibit a large specific capacity and high safety at a low cost is required.

To improve the performance of LIBs, transition metal oxides, phosphides, sulfides and various other materials have been widely used as cathode materials. Among these materials, transition metal oxides are considered potential cathode materials due to their physical and chemical properties, which help to obtain high specific capacities and an excellent cycling performance [13]. Vanadium pentoxide (V₂O₅), a potential transition metal oxide, has

garnered great interest due to its mainly variable oxidation states (V^{2+} , V^{3+} , V^{4+} and V^{5+}). V^{5+} is the most stable oxidation state of V_2O_5 , and it is widely studied as a cathode material due to its low-cost, easy and scalable synthesis and high working voltage [14–16]. In addition, V_2O_5 has a layered crystal structure which allows it to accommodate the volume change during Li^+ insertion/extraction efficiently, resulting in enhanced electrochemical performances [17]. The theoretical capacity of V_2O_5 is deeply affected by the amount of intercalated Li^+ ions in the crystal structure, which eventually form $Li_xV_2O_5$ ($0 < x < 2$). However, the x value can be increased until $2 < x < 3$ due to the continuous Li^+ ion insertion at higher voltages [18,19]. As a cathode material for LIBs, the theoretical capacities of V_2O_5 of $\sim 294 \text{ mAh g}^{-1}$ and $\sim 440 \text{ mAh g}^{-1}$ can be obtained based on the intercalation of two and three Li^+ ions, respectively, which are nearly three times higher than the theoretical capacity of $LiCoO_2$ ($\sim 140 \text{ mAh g}^{-1}$) [14]. Despite all these advantages, V_2O_5 still suffers from fast capacity fading due to the low lithium-ion diffusion efficiency, insufficient contact areas and poor structural stability [20–22]. For obtaining an enhanced electrochemical performance, higher electrode/electrolyte interfaces and a better accommodation ability of the strain upon volume change during lithiation/de-lithiation, nanostructured materials also possess advantages. Numerous nanostructured V_2O_5 samples have been reported, such as nanoparticles [23], micro/nanosphere [24–26], nanosheets [27–29], nanorods [30], nanotubes [31] and nanowires [32], to alleviate the kinetic limitations when employed as a cathode material for LIB.

Since metal-organic frameworks are the new class of porous inorganic-organic materials, demonstrating an alterable high specific surface area, framework topologies, active-metal sites, a crystalline structure and tunable pore sizes, they have attracted much attention for their promising applications in batteries and supercapacitors [33,34]. Therefore, in this work, we have synthesized oval-shaped V_2O_5 nanoparticles by using a simple and facile hydrothermal synthesis method. To synthesize a vanadium-based metal-organic framework, terephthalic acid as an organic moiety and vanadium acetylacetonate as a metal precursor were used. It is believed that the MOF provides a skeleton for the growth of an oval-shaped nanostructure. When V_2O_5 was applied as a cathode material for LIBs, it exhibited remarkable electrochemical performances.

2. Materials and Methods

2.1. Material Synthesis

Oval-shaped V_2O_5 nanoparticles were successfully synthesized using the facile hydrothermal synthesis method. Firstly, 2 mmol each of vanadium acetylacetonate (Sigma Aldrich, Saint Louis, MO, USA, 97%) and terephthalic acid (SRL, Mumbai, India, 98%) were dissolved in 60 mL of isopropanol with continuous stirring. The terephthalic acid is used here as an organic moiety to form a metal-organic framework. After continuous stirring for 45 min, the obtained homogeneous solution was then transferred to a Teflon-lined stainless-steel autoclave and heated at $180 \text{ }^\circ\text{C}$ for 12 h. After natural cooling, the obtained product was centrifuged and washed with distilled water/ethanol several times. After drying the sample at $75 \text{ }^\circ\text{C}$ overnight, the calcination was performed at $450 \text{ }^\circ\text{C}$ for 1 h in an air atmosphere.

2.2. Materials Characterisation

To discover the calcination temperature, the thermal analysis of the as-prepared sample was recorded using thermogravimetric/differential thermal analysis (TG/DTA) on a Shimadzu DTG 60 instrument (Shimadzu, Kyoto, Japan) from room temperature to $700 \text{ }^\circ\text{C}$ under an air atmosphere. The crystallinity, purity, particle sizes and morphology of the calcined sample were investigated using X-ray diffraction analysis (XRD, Bruker, D8 Discover High Resolution X-Ray Diffractometer with $Cu \text{ K}\alpha$ radiation, $\lambda = 1.5406 \text{ \AA}$, Karlsruhe, Germany) and field-emission transmission electron microscopy (FE-TEM, Philips TecnaiF20 at 200 kV, Philips, Amsterdam, The Netherlands). The elemental distribution analysis of

the calcined sample was carried out by energy-dispersive X-ray spectrometry (EDX, Mode: JSM 6610LV, JEOL, Tokyo, Japan).

2.3. Electrode Fabrication

The testing electrodes were fabricated by mixing the active material of V_2O_5 (75 wt %), Ketjen black (15 wt %) and polyvinylidene fluoride (PVDF) (10 wt %) using an N-methyl 2-pyrrolidone (NMP) solvent. Then, the mixture was cast onto the aluminium foil (current collector) using a doctor blade. After drying the slurry in a vacuum oven at 120 °C overnight, it was hot-pressed using a twin roller hot press for better adhesion between the slurry and the current collector. The electrochemical cells were assembled using lithium metal foil (reference electrode), glass fiber (separator) and 1M $LiPF_6$ with a volumetric ratio of EC:DMC of 1:1 (electrolyte) in an argon-filled glove box. The electrochemical properties of the assembled half-cell were investigated on a Wonatech WBCS 3000 electrochemical workstation within the potential window of 1.5–4.5 V vs. Li^+/Li at different current densities.

3. Results

3.1. Physicochemical Analysis

As can be seen from Figure 1, a total of 58% of weight loss was observed in the TG curve within the temperature range of 200–400 °C, which can be ascribed to the removal of the functional groups of co-ordinated molecules and the carbon skeleton presented in the precursors. Since there was no significant weight loss observed after 400 °C until 700 °C, the as-prepared sample was calcined at 450 °C.

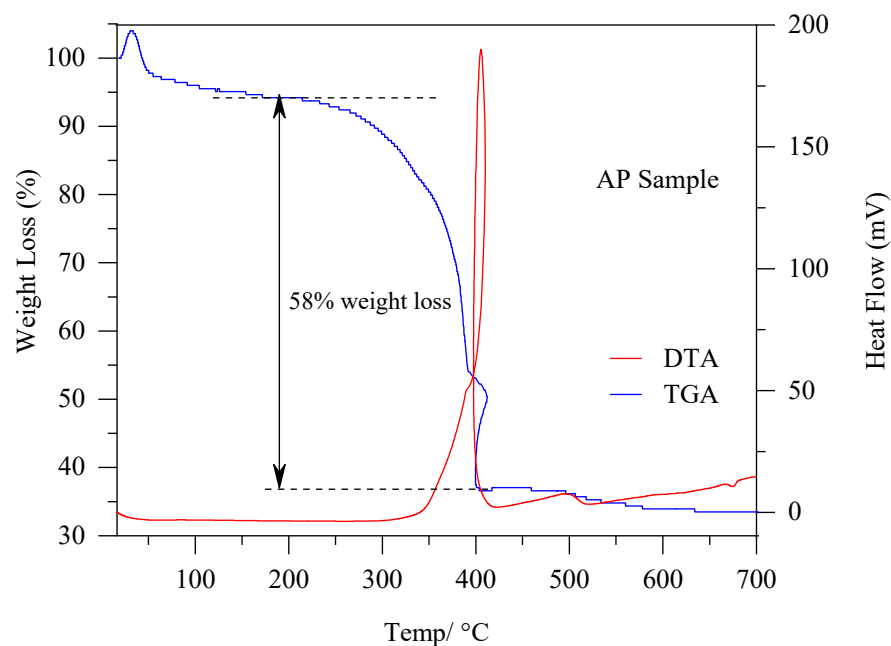


Figure 1. TG-DTA curves of the as-prepared V_2O_5 sample with the layered crystal structure.

To further confirm the formation of V_2O_5 after calcination at 450 °C, powder X-ray diffraction was performed. The XRD pattern, along with the crystal structure of V_2O_5 , is demonstrated in Figure 2a. All of the diffraction peaks were exactly matched with the standard JCPDS data (card no. 00-041-1426, orthorhombic crystal system and Pmmn space group). It can be noticed that the obtained diffraction peaks are highly intense and sharp, which confirmed the crystallinity of the sample without any extra impurity peak. The layered crystal structure of V_2O_5 is also depicted in the inset of Figure 2a.

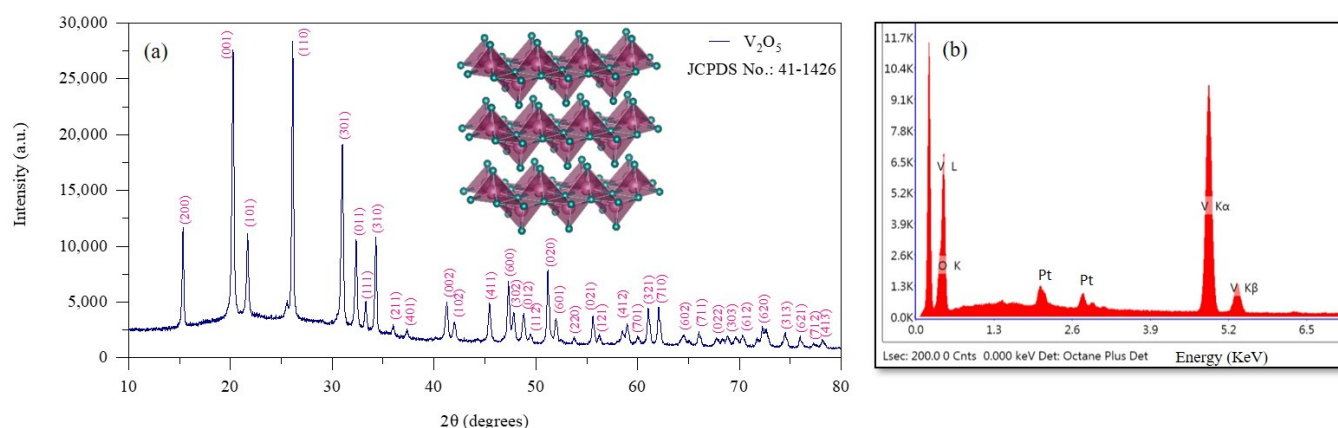


Figure 2. (a) Powder XRD patterns and (b) EDS spectra of the as-prepared V_2O_5 sample with the layered crystal structure.

To further investigate the morphological details of the calcined V_2O_5 sample, FE-TEM was employed, and the obtained results are displayed in Figure 3. As can be seen from Figure 3a,b, the mixed size and shape of the nanoparticles, including the oval-shaped nanoparticles with an average size of ~ 50 – 250 nm, are observed throughout the sample. More importantly, there is also less agglomeration, which may be due to the use of the MOF. The typical HR-TEM image in Figure 3b clearly shows lattice fringes with d-spacings of 0.57 nm and 0.34 nm, which correspond to the (200) and (110) planes of the sample. The obtained planes are perfectly matched with the XRD peaks, indicating the high purity of the sample. To further investigate the elemental distribution in the calcined V_2O_5 sample, energy dispersive spectroscopy (EDS) analysis was also performed, and the result is displayed in Figure 2b. The obtained EDS spectra revealed the presence of vanadium (V) and oxygen (O) elements in the sample without any other impurity, which further indicates the fabrication of a pure V_2O_5 sample.

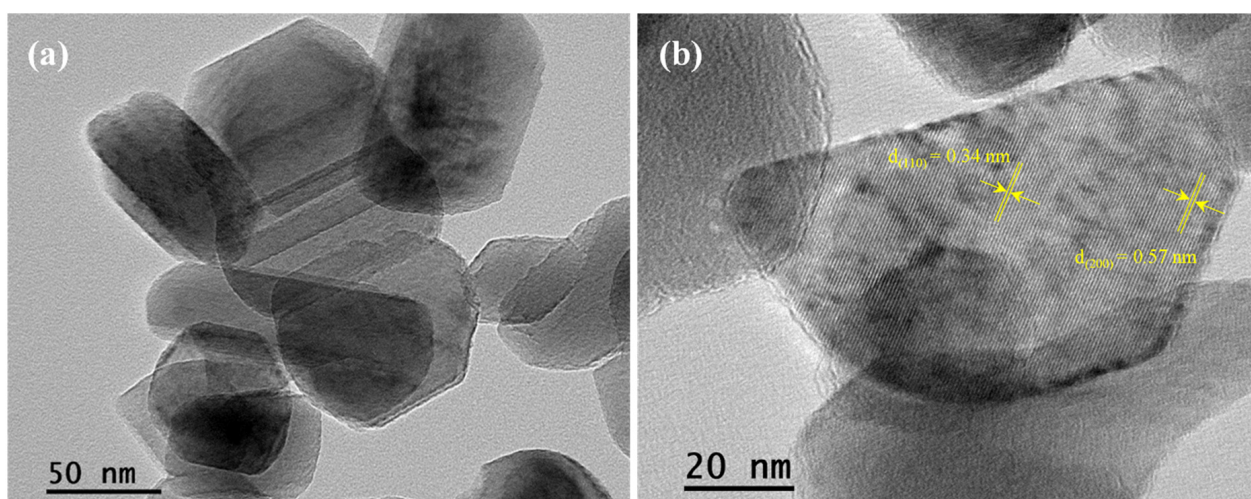


Figure 3. (a) FE-TEM image and (b) HR-TEM image of the calcined oval-shaped V_2O_5 nanoparticles sample.

3.2. Electrochemical Performances

To further investigate the electrochemical performances of V_2O_5 as a cathode material, the galvanostatic charge/discharge measurement was first examined at a current density of 250 mA g^{-1} , and the obtained result is displayed in Figure 4a. During the first discharge cycle, numerous irreversible reduction plateaus can be seen, which correspond to the formation of a solid electrolyte interface (SEI) layer as well as multistep electrochemical

reactions between Li^+ and V_2O_5 [35]. From the second cycle onwards, the shape of curves became similar without multistep reduction plateaus being observed in any discharge cycle, indicating the reversible electrochemical reactions within the electrode. The observed significant change in the charge–discharge profiles can be attributed merely to their different electrochemical responses against applied voltages. The V_2O_5 cathode delivered initial discharge/charge capacities of 422.9 and 356.4 mAh g^{-1} , respectively, with a corresponding initial coulombic efficiency of 84.2%. However, as can be noticed, the electrode can deliver a discharge/charge capacity of 267.5/263.9 mAh g^{-1} after 10 cycles, with a coulombic efficiency of ~99%.

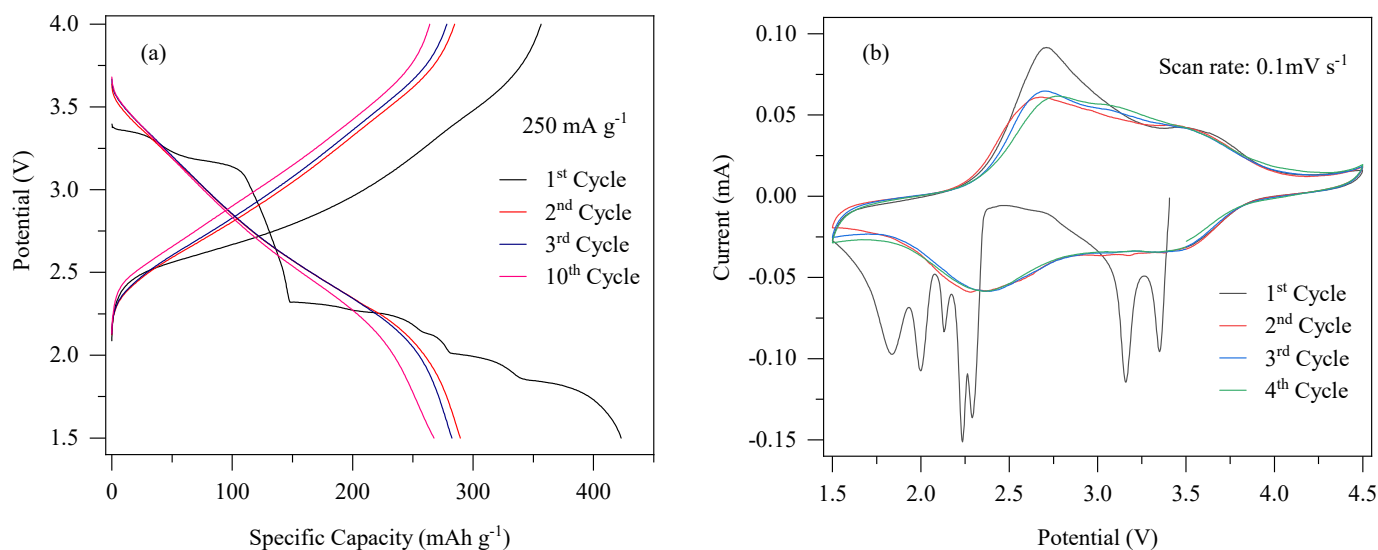
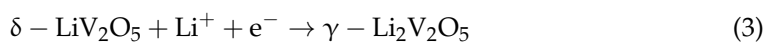
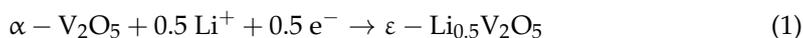


Figure 4. (a) Charge–discharge profile under the voltage range of 1.5–4.0 V at 250 mA g^{-1} and (b) cyclic voltammetry curves at a scan rate of 0.1 mV s^{-1} of the oval-shaped V_2O_5 nanoparticles electrode.

The cyclic voltammetry (CV) profiles of the V_2O_5 cathode at a scan rate of 0.1 mV s^{-1} are depicted in Figure 4b within the voltage range of 1.5–4.0 V. The first cathodic scan exhibits the multiple irreversible reduction peaks at ~3.35 V, ~3.16 V, ~2.29 V, ~2.23 V, ~2.0 V and ~1.83 V, as observed in the first discharge cycle (Figure 3a), which can be attributed to the multistep lithiation of the V_2O_5 electrode and the formation of the solid electrolyte interface layer. It is well known that the phase transformation occurred during lithiation from $\alpha\text{-V}_2\text{O}_5$ to $\varepsilon\text{-Li}_{0.5}\text{V}_2\text{O}_5$, $\delta\text{-LiV}_2\text{O}_5$ and then to $\gamma\text{-Li}_2\text{V}_2\text{O}_5$, respectively [35–37]. However, in the subsequent discharge scans, these multiple reduction peaks completely vanished, and the two main broad peaks located at ~2.4 V and ~3.5 V are observed, which can be attributed to the pseudocapacitive behavior of the V_2O_5 cathode [20]. On the other hand, the two major peaks located at ~2.7 V and ~3.7 V can be seen during the anodic scan, which can be attributed to the reversible phase transformation of V_2O_5 . More importantly, from the second cycle onwards, the two pairs of redox peaks between the voltage window of ~2.0–4.0 V can be observed, which correspond to the reversible Li^+ insertion/de-insertion within the electrode [36]. Generally, V_2O_5 accepts two Li^+ ions during the discharge and $\text{Li}_2\text{V}_2\text{O}_5$ forms, which converts back to layered V_2O_5 after the removal of Li^+ ions during charging. The corresponding reactions can be as follows: [37]



To further examine the structural stability, the cycling performances were also tested at two different current densities and 250 mA g^{-1} , as shown in Figure 5a. It can be seen

that the electrode demonstrates stable cycling performances with the discharge capacities of 169.3 mAh g^{-1} at 133 mA g^{-1} and 150.7 mAh g^{-1} at 250 mA g^{-1} after 50 cycles. Thus, the oval-shaped V_2O_5 nanoparticles electrode showed excellent capacity retention and a stable cycle life during the charge/discharge reactions, which is possibly due to the unique nanostructure, imparting a high surface area and numerous path channels for the insertion/de-insertion of Li^+ ions. Moreover, the rate capability of the V_2O_5 cathode material was also investigated at numerous current densities, and the results are displayed in Figure 5b. It can be noticed that the electrode is cycled for 10 cycles at each current density. The electrode delivered discharge capacities of 445.1, 268.15, 198.6 and 128.1 mAh g^{-1} at the current densities of 133, 266, 532 and 1330 mA g^{-1} , respectively. In addition, when the electrode was reversed back to the lower current density of 133 mA g^{-1} after 50 cycles of charge/discharge between the lower and higher current densities, it regained a capacity that was similar to the previous capacity, which confirmed the structural stability of the oval-shaped V_2O_5 nanoparticles cathode.

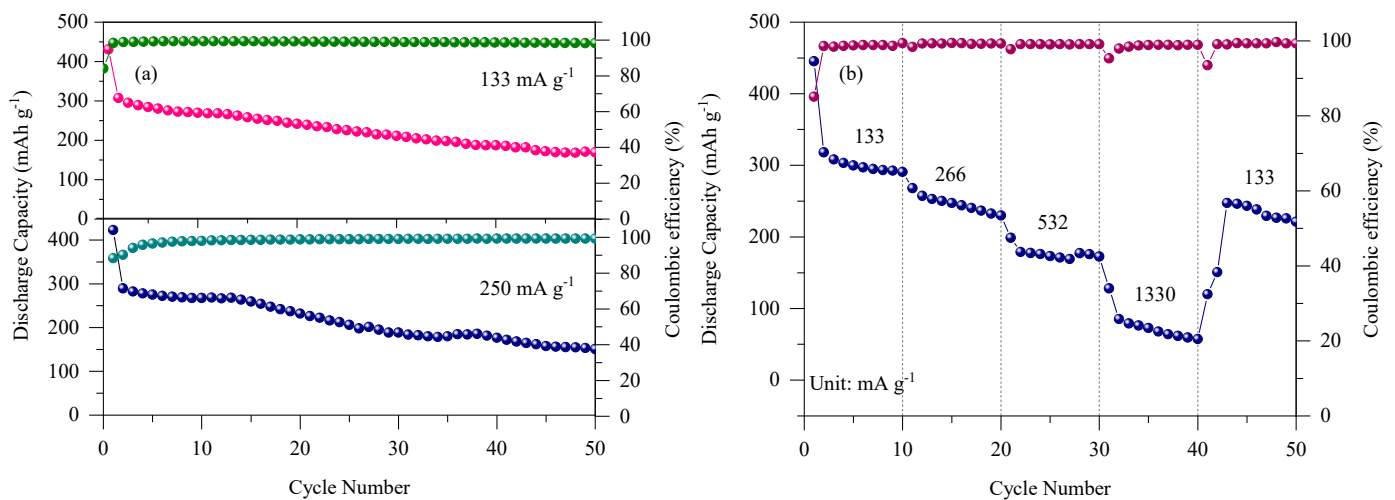


Figure 5. (a) Cycling performance at the constant current densities of 133 and 250 mA g^{-1} until 50 cycles and (b) the capacity retention at various current densities from 133 to 1330 mA g^{-1} of the oval-shaped V_2O_5 nanoparticles electrode.

Since various research articles have already been reported in the literature, we have prepared an electrochemical performance comparison table between the current oval-shaped V_2O_5 nanoparticle electrode and the previously reported pure and composite V_2O_5 electrode materials based on numerous nanostructures. It is concluded from Table 1 that the oval-shaped V_2O_5 nanoparticle electrode provides a comparable electrochemical performance and can be considered a potential cathode material for LIB.

Table 1. Electrochemical performance comparison between the current oval-shaped V_2O_5 nanoparticle electrode and the previously reported pure and composite V_2O_5 electrode materials based on numerous nanostructures.

Material	Synthesis Method	Nanostructure	Electrochemical Performance (Dis. Capacity/Cycle Number/Rate)	Ref.
V_2O_5	The polymer-assisted chemical solution method	Network	99 mAh g^{-1} /100 cycles/1 A g^{-1}	[38]
V_2O_5	Solvothermal	Sheets	140 mAh g^{-1} /100 cycles/0.1C	[39]
V_2O_5 /MWCNT		Particles	190 mAh g^{-1} /100 cycles/0.1C	
V_2O_5	Hydrothermal	Nanobelts	168 mAh g^{-1} /50th cycles/50 mA g^{-1}	[40]
V_2O_5	The ultrasonic method with subsequent thermal decomposition.	Nanosheets	179.5 mAh g^{-1} /50 cycles/1C	[37]
V_2O_5		Nanoparticles	106.1 mAh g^{-1} /50 cycles/1C	
V_2O_5	Hydrothermal/annealing	SLMNSs	202 mAh g^{-1} /50 cycles/100 mA g^{-1}	[41]
V_2O_5		Nanoribbons	131 mAh g^{-1} /50 cycles/100 mA g^{-1}	
V_2O_5	Microwave-assisted hydrothermal synthesis	Separate nanorods	112.6 mAh g^{-1} /50 Cycles/100 mA g^{-1}	[42]
V_2O_5		Nanorods assemblies	191.6 mAh g^{-1} /50 cycles/100 mA g^{-1}	
V_2O_5 -SnO ₂	Solvothermal	Double-shelled nanocapsules	174 mAh g^{-1} /50 Cycles/100 mA g^{-1}	[20]
V_2O_5	Hydrothermal	Nanowire	126 mAh g^{-1} /100 Cycles/100 mA g^{-1}	[43]
V_2O_5 /rGO		Quantum dots	212 mAh g^{-1} /100 Cycles/100 mA g^{-1}	
V_2O_5	Solvothermal	Hollow microspheres	125 mAh g^{-1} /100 Cycles/1 C	[44]
V_2O_5	Solvothermal	Nanoparticles	91.40 mAh g^{-1} /100 Cycles/50 mA g^{-1}	[45]
V_2O_5	Hydrothermal	Nanoflakes/Nanoparticles	139 mAh g^{-1} /50 Cycles/15 mA g^{-1}	[46]
V_2O_5	Hydrothermal	Oval-shaped Nanoparticle	169.3 mAh g^{-1} /50 cycles/133 mA g^{-1}	This work
V_2O_5			150.7 mAh g^{-1} /50 cycles/250 mA g^{-1}	

4. Conclusions

This work demonstrates a metal-organic framework that fabricated an oval-shaped V_2O_5 cathode material by using a simple and facile hydrothermal synthesis method. It is believed that the obtained unique nanostructure of the V_2O_5 electrode may provide a high surface area and numerous channels for Li^+ insertion/de-insertion, resulting in improved electrochemical performances. When applied as a cathode material, the electrode exhibits discharge capacities of 169.3 mAh g^{-1} at 133 mA g^{-1} and 150.7 mAh g^{-1} at 250 mA g^{-1} after 50 cycles and 57.5 mAh g^{-1} at a high current density of 1330 mA g^{-1} after 40 cycles. The obtained electrochemical performances showed that the oval-shaped V_2O_5 electrode is a potential cathode material for LIBs, and the current synthetic strategy can be also extended to the fabrication of other electrode materials.

Author Contributions: Conceptualization, J.S. and K.H.; methodology, J.S. and K.H.; software, J.S., K.H., M.S.A. and A.K.R.; validation, J.S., K.H., M.S.A. and A.K.R.; formal analysis, J.S. and K.H.; investigation, J.S., J.K., K.H., Y.C. and A.K.R.; data curation, J.S., K.H., Y.C., J.K. and A.K.R.; writing—original draft preparation, J.S., K.H., J.K. and A.K.R.; writing—review and editing, Y.C., M.S.A. and A.K.R.; visualization, Y.C. and A.K.R.; supervision, Y.C. and A.K.R.; funding acquisition, Y.C. and A.K.R. All authors have read and agreed to the published version of the manuscript.

Funding: This work was mainly supported by the Council of Scientific and Industrial Research (CSIR) Research Grant (File No. 01(3015)/21/EMR-II). This work was also partially supported by the Basic Science Research Program through the National Research Foundation of Korea (NRF) funded by the Ministry of Education (2021R111A3057918).

Institutional Review Board Statement: Not applicable.

Informed Consent Statement: Not applicable.

Data Availability Statement: Not applicable.

Acknowledgments: One of the authors (Jay Singh) would like to thank the CSIR, New Delhi, for the award of a senior research fellowship. Alok Kumar Rai is grateful to the University Grants Commission (UGC) for the position and funding support under the UGC-FRP scheme (FRP ID: 57304).

Conflicts of Interest: The authors declare no conflict of interest.

References

1. Nitta, N.; Wu, F.; Lee, J.T.; Yushin, G. Li-ion battery materials: Present and future. *Mater. Today* **2015**, *18*, 252–264. [[CrossRef](#)]
2. Tian, B.; Kempa, T.J.; Lieber, C.M. Single nanowire photovoltaics. *Chem. Soc. Rev.* **2009**, *38*, 16–24. [[CrossRef](#)] [[PubMed](#)]
3. Hu, B.; Cheng, H.; Huang, C.; Aslam, M.K.; Liu, L.; Xu, C.; Chen, P.; Yu, D.; Chen, C. The controlled study of surfactants on the morphologies of three-dimensional turbine-like V_2O_5 for the application of high performance lithium ion storage. *Solid State Ionics* **2019**, *342*, 115059. [[CrossRef](#)]
4. Dou, Y.; Liang, X.; Gao, G.; Wu, G. Template-free synthesis of porous V_2O_5 yolk-shell microspheres as cathode materials for lithium ion batteries. *J. Alloys Compd.* **2018**, *735*, 109–116. [[CrossRef](#)]
5. Chen, M.; Liang, X.; Yin, J.; Chen, Q.; Xia, X. Graphene foam supported V_2O_5 /N-C core/shell arrays as advanced cathode for lithium-ion storage. *J. Alloys Compd.* **2018**, *735*, 2022–2029. [[CrossRef](#)]
6. Wang, J.; Sun, X. Understanding and recent development of carbon coating on $LiFePO_4$ cathode materials for lithium-ion batteries. *Energy Environ. Sci.* **2012**, *5*, 5163–5185. [[CrossRef](#)]
7. Yadav, G.G.; David, A.; Zhu, H.; Caruthers, J.; Wu, Y. Microemulsion-based synthesis and electrochemical evaluation of different nanostructures of $LiCoO_2$ prepared through sacrificial nanowire templates. *Nanoscale* **2014**, *6*, 860–866. [[CrossRef](#)]
8. Cai, Y.; Huang, Y.; Wang, X.; Jia, D.; Pang, W.K.; Guo, Z.; Du, Y.; Tang, X. Facile synthesis of $LiMn_2O_4$ octahedral nanoparticles as cathode materials for high capacity lithium ion batteries with long cycle life. *J. Power Sources* **2015**, *278*, 574–581. [[CrossRef](#)]
9. Haris, M.; Atiq, S.; Abbas, S.M.; Mahmood, A.; Ramay, S.M.; Naseem, S. Acetylene black coated V_2O_5 nanocomposite with stable cyclability for lithium-ion batteries cathode. *J. Alloys Compd.* **2018**, *732*, 518–523. [[CrossRef](#)]
10. Chen, A.; Li, C.; Zhang, C.; Li, W.; Yang, Q. The mechanical hybrid of V_2O_5 microspheres/graphene as an excellent cathode for lithium-ion batteries. *J. Solid State Electrochem.* **2022**, *26*, 729–738. [[CrossRef](#)]
11. Lang, X.; Li, Y.; Cai, K.; Li, L.; Chen, D.; Zhang, Q. Influence of Sulfur-Modified Vanadium Pentoxide by Solid Phase Sintering Method on Electrochemical Performance of Cathode Materials for Lithium-Ion Batteries. *Energy Technol.* **2019**, *7*, 1800808. [[CrossRef](#)]
12. Zeng, J.; Huang, J.; Liu, J.; Xie, T.; Peng, C.; Lu, Y.; Lu, P.; Zhang, R.; Min, J. Self-assembly of single layer V_2O_5 nanoribbon/graphene heterostructures as ultrahigh-performance cathode materials for lithium-ion batteries. *Carbon* **2019**, *154*, 24–32. [[CrossRef](#)]
13. Shashank, M.; Alharthi, F.A.; Alsalmeh, A.; Al-Zaqri, N.; Nagaraju, G. Ag decorated V_2O_5 nanorods as cathode material for lithium-ion battery. *J. Mater. Sci. Mater. Electron.* **2020**, *31*, 14279–14286. [[CrossRef](#)]
14. Yue, Y.; Liang, H. Micro- and Nano-Structured Vanadium Pentoxide (V_2O_5) for Electrodes of Lithium-Ion Batteries. *Adv. Energy Mater.* **2017**, *7*, 1602545. [[CrossRef](#)]
15. Pan, A.Q.; Wu, H.B.; Zhang, L.; Lou, X.W.D. Uniform V_2O_5 nanosheet-assembled hollow micro flowers with excellent lithium storage properties. *Energy Environ. Sci.* **2013**, *6*, 1476–1479. [[CrossRef](#)]
16. Chen, P.; Zheng, G.; Guo, G.; Wang, Z.; Tang, J.; Li, S.; Wen, Z.; Ji, S.; Sun, J. Ce-doped V_2O_5 microspheres with improved electrochemical performance for high-power rechargeable lithium ion batteries. *J. Alloys Compd.* **2019**, *784*, 574–583. [[CrossRef](#)]
17. Tang, Y.; Rui, X.; Zhang, Y.; Lim, T.M.; Dong, Z.; Hng, H.H.; Chen, X.; Yan, Q.; Chen, Z. Vanadium pentoxide cathode materials for high-performance lithium-ion batteries enabled by a hierarchical nanoflower structure via an electrochemical process. *J. Mater. Chem. A* **2013**, *1*, 82–88. [[CrossRef](#)]
18. Li, M.; Kong, F.; Wang, H.; Li, G. Synthesis of vanadium pentoxide (V_2O_5) ultralong nanobelts via an oriented attachment growth mechanism. *CrystEngComm* **2011**, *13*, 5317–5320. [[CrossRef](#)]
19. Zhai, T.; Liu, H.; Li, H.; Fang, X.; Liao, M.; Li, L.; Zhou, H.; Koide, Y.; Bando, Y.; Golberg, D. Centimeter-Long V_2O_5 Nanowires: From Synthesis to Field-Emission, Electrochemical, Electrical Transport, and Photoconductive Properties. *Adv. Mater.* **2010**, *22*, 2547–2552. [[CrossRef](#)]
20. Liu, J.; Xia, H.; Xue, D.; Lu, L. Double-Shelled Nanocapsules of V_2O_5 -Based Composites as High-Performance Anode and Cathode Materials for Li Ion Batteries. *J. Am. Chem. Soc.* **2009**, *131*, 12086–12087. [[CrossRef](#)]
21. Mai, L.; Dong, F.; Xu, X.; Luo, Y.; An, Q.; Zhao, Y.; Pan, J.; Yang, J. Cucumber-Like V_2O_5 /poly(3,4-ethylenedioxythiophene) & MnO_2 Nanowires with Enhanced Electrochemical Cyclability. *Nano Lett.* **2013**, *13*, 740–745. [[PubMed](#)]
22. Liu, Y.; Gao, G.; Liang, X.; Wu, G. Nanofibers of V_2O_5 /C@MWCNTs as the cathode material for lithium-ion batteries. *J. Solid State Electrochem.* **2018**, *22*, 2385–2393. [[CrossRef](#)]
23. Liu, X.; Zeng, J.; Yang, H.; Zhou, K.; Pan, D. V_2O_5 -Based nanomaterials: Synthesis and their applications. *RSC Adv.* **2018**, *8*, 4014–4031. [[CrossRef](#)]
24. Bin Wu, H.; Pan, A.; Hng, H.H.; Lou, X.W. Template-Assisted Formation of Rattle-type V_2O_5 Hollow Microspheres with Enhanced Lithium Storage Properties. *Adv. Funct. Mater.* **2013**, *23*, 5669–5674. [[CrossRef](#)]

25. Pan, A.; Bin Wu, H.; Yu, L.; Lou, X.W. Template-Free Synthesis of VO₂ Hollow Microspheres with Various Interiors and Their Conversion into V₂O₅ for Lithium-Ion Batteries. *Angew. Chem.* **2013**, *125*, 2282–2286. [[CrossRef](#)]
26. Ma, Y.; Huang, A.; Zhou, H.; Ji, S.; Zhang, S.; Li, R.; Yao, H.; Cao, X.; Jin, P. Template-free formation of various V₂O₅ hierarchical structures as cathode materials for lithium-ion batteries. *J. Mater. Chem. A* **2017**, *5*, 6522–6531. [[CrossRef](#)]
27. Zeng, Y.; Gao, G.; Wu, G.; Yang, H. Nanosheet-structured vanadium pentoxide thin film as a carbon- and binder-free cathode for lithium-ion battery applications. *J. Solid State Electrochem.* **2015**, *19*, 3319–3328. [[CrossRef](#)]
28. Qi, Y.; Qin, K.; Jian, Z.; Yang, X.; Jin, W.; Tan, Y.; Zou, Y.; Chen, W. Ag-functionalized exfoliated V₂O₅ nanosheets: A flexible and binder-free cathode for lithium-ion batteries. *J. Mater. Sci.* **2019**, *54*, 12713–12722. [[CrossRef](#)]
29. Cheng, J.; Gu, G.; Guan, Q.; Razal, J.M.; Wang, Z.; Li, X.; Wang, B. Synthesis of a porous sheet-like V₂O₅-CNT nanocomposite using an ice-templating ‘bricks-and-mortar’ assembly approach as a high capacity, long cycle life cathode material for lithium-ion batteries. *J. Mater. Chem.* **2016**, *4*, 2729–2737. [[CrossRef](#)]
30. Wang, H.-G.; Ma, D.-L.; Huang, Y.; Zhang, X.-B. Electrospun V₂O₅ Nanostructures with Controllable Morphology as High-Performance Cathode Materials for Lithium-Ion Batteries. *Chem. A Eur. J.* **2012**, *18*, 8987–8993. [[CrossRef](#)]
31. Yao, X.; Guo, G.; Li, P.Z.; Luo, Z.Z.; Yan, Q.; Zhao, Y. Scalable synthesis of honeycomblike V₂O₅/carbon nanotube networks as enhanced cathodes for lithium-ion batteries. *ACS Appl. Mater. Interfaces* **2017**, *9*, 42438–42443. [[CrossRef](#)] [[PubMed](#)]
32. Mai, L.; Tian, X.; Xu, X.; Chang, L.; Xu, L. Nanowire Electrodes for Electrochemical Energy Storage Devices. *Chem. Rev.* **2014**, *114*, 11828–11862. [[CrossRef](#)] [[PubMed](#)]
33. Janiak, C.; Vieth, J.K. MOFs, MILs and more: Concepts, properties and applications for porous coordination networks (PCNs). *New J. Chem.* **2010**, *34*, 2366–2388. [[CrossRef](#)]
34. Ni, Z.; Masel, R.I. Rapid Production of Metal–Organic Frameworks via Microwave-Assisted Solvothermal Synthesis. *J. Am. Chem. Soc.* **2006**, *128*, 12394–12395. [[CrossRef](#)]
35. Wang, C.; Zhang, L.; Al-Mamun, M.; Dou, Y.; Liu, P.; Su, D.; Wang, G.; Zhang, S.; Wang, D.; Zhao, H. A Hollow-Shell Structured V₂O₅ Electrode-Based Symmetric Full Li-Ion Battery with Highest Capacity. *Adv. Energy Mater.* **2019**, *9*, 1900909. [[CrossRef](#)]
36. Zhang, H.; Rong, Y.; Jia, W.; Chai, H.; Cao, Y. Simple solvent-free synthesis of rod-like Cu-doped V₂O₅ for high storage capacity cathode materials of lithium-ion batteries. *J. Alloys Compd.* **2019**, *802*, 139–145. [[CrossRef](#)]
37. Huang, J.; Qiao, X.; Xu, Z.; Cao, L.; Ouyang, H.; Li, J.; Wang, R. V₂O₅ self-assembled nanosheets as high stable cathodes for Lithium-ion batteries. *Electrochim. Acta* **2016**, *191*, 158–164. [[CrossRef](#)]
38. Xu, Y.; Dunwell, M.; Fei, L.; Fu, E.; Lin, Q.; Patterson, B.; Yuan, B.; Deng, S.; Andersen, P.; Luo, H.; et al. Two-Dimensional V₂O₅ Sheet Network as Electrode for Lithium-Ion Batteries. *ACS Appl. Mater. Interfaces* **2014**, *6*, 20408–20413. [[CrossRef](#)]
39. Partheeban, T.; Kesavan, T.; Vivekanantha, M.; Sasidharan, M. One-pot solvothermal synthesis of V₂O₅/MWCNT composite cathode for Li-ion batteries. *Appl. Surf. Sci.* **2019**, *493*, 1106–1114. [[CrossRef](#)]
40. Niu, C.; Li, J.; Jin, H.; Shi, H.; Zhu, Y.; Wang, W.; Cao, M. Self-template processed hierarchical V₂O₅ nanobelts as cathode for high performance lithium ion battery. *Electrochim. Acta* **2015**, *182*, 621–628. [[CrossRef](#)]
41. Liu, P.; Zhu, K.; Bian, K.; Xu, Y.; Zhang, F.; Zhang, W.; Zhang, J.; Huang, W. 3D hierarchical porous sponge-like V₂O₅ micro/nano-structures for high-performance Li-ion batteries. *J. Alloys Compd.* **2018**, *765*, 901–906. [[CrossRef](#)]
42. Pan, J.; Li, M.; Luo, Y.; Wu, H.; Zhong, L.; Wang, Q.; Li, G. Microwave-assisted hydrothermal synthesis of V₂O₅ nanorods assemblies with an improved Li-ion batteries performance. *Mater. Res. Bull.* **2016**, *74*, 90–95. [[CrossRef](#)]
43. Han, C.; Yan, M.; Mai, L.; Tian, X.; Xu, L.; Xu, X.; An, Q.; Zhao, Y.; Ma, X.; Xie, J. V₂O₅ quantum dots/graphene hybrid nanocomposite with stable cyclability for advanced lithium batteries. *Nano Energy* **2013**, *2*, 916–922. [[CrossRef](#)]
44. Shan, Y.; Xu, L.; Hu, Y.; Jiang, H.; Li, C. Internal-diffusion controlled synthesis of V₂O₅ hollow microspheres for superior lithium-ion full batteries. *Chem. Eng. Sci.* **2019**, *200*, 38–45. [[CrossRef](#)]
45. Zhang, Y.; Zou, Z.; Liu, J.; Zhang, S.; Zhang, H. Effect of Ga doping on structure and properties of V₂O₅ lithium-ion batteries. *Mater. Technol.* **2020**, *35*, 887–895. [[CrossRef](#)]
46. Cao, L.; Kou, L.; Li, J.; Huang, J.; Yang, J.; Wang, Y. Nitrogen-doped carbon-coated V₂O₅ nanocomposite as cathode materials for lithium-ion battery. *J. Mater. Sci.* **2018**, *53*, 10270–10279. [[CrossRef](#)]